PERGAMON

International Journal of Solids and Structures 39 (2002) 6311–6337

INTERNATIONAL JOURNAL OF SOLIDS and STRUCTURES

www.elsevier.com/locate/ijsolstr

Propagation of a penny-shaped fluid-driven fracture in an impermeable rock: asymptotic solutions

A.A. Savitski, E. Detournay *

Department of Civil Engineering, University of Minnesota, 500 Pillsbury Drive SE, Minneapolis, MN 55455, USA

Received 1 April 2002; received in revised form 29 August 2002

Abstract

This paper presents an analysis of the propagation of a penny-shaped hydraulic fracture in an impermeable elastic rock. The fracture is driven by an incompressible Newtonian fluid injected from a source at the center of the fracture. The fluid flow is modeled according to lubrication theory, while the elastic response is governed by a singular integral equation relating the crack opening and the fluid pressure. It is shown that the scaled equations contain only one parameter, a dimensionless toughness, which controls the regimes of fracture propagation. Asymptotic solutions for zero and large dimensionless toughness are constructed. Finally, the regimes of fracture propagation are analyzed by matching the asymptotic solutions with results of a numerical algorithm applicable to arbitrary toughness.

Keywords: Fracture; Asymptotic; Propagation; Elastic

1. Introduction

This paper deals with hydraulic fracturing, a technique mainly used in the petroleum industry to enhance the recovery of oil and gas from underground hydrocarbon reservoirs. Other applications include (but are not limited to) underground disposal of liquid toxic waste, determination of in situ stresses in rock, and creation of geothermal energy reservoirs, see the review by Mendelsohn (1984).

Hydraulic fracturing consists of injecting a viscous fluid into a well under high pressure to initiate and propagate a fracture. The design of a treatment relies on the ability to predict the opening and the size of the fracture as well as the pressure of the fracturing fluid, as a function of the properties of the rock and the fluid. However, in view of the great uncertainty in the in situ conditions, it is of particular importance to identify the key dimensionless parameters and to understand the dependence of the hydraulic fracturing process on these parameters. In that respect, the availability of solutions for idealized situations is especially valuable. The construction of such solutions, for the particular case of a penny-shaped fluid-driven fracture in an elastic medium, is one of the topics of this paper.

* Corresponding author. Tel.: +1-612-625-3043; fax: +1-612-626-7750.
E-mail addresses: detou001@umn.edu, detou001@tc.umn.edu (E. Detournay).

0020-7683/02/$ - see front matter
PII: S0020-7683(02)00492-4

Since the pioneering work by Khristianovic and Zheltov (1955), there have been numerous contributions on the modeling of fluid-driven fractures. The early efforts naturally focused on analytical solutions for fractures of simple geometry, either straight in plane strain or penny-shaped (Khristianovic and Zheltov, 1955; Barenblatt, 1956; Perkins and Kern, 1961; Geertsma and de Klerk, 1969; Nordgren, 1972; Abé et al., 1976; Geertsma and Haafkens, 1979; Advani et al., 1987). All these solutions are approximate, however, as they contain strong assumptions about either the opening or the pressure field. Behind such simplifications lies the difficulty of solving the coupled non-linear integro-differential equations that govern the problem in question.

In recent years, the limitations of analytical models have shifted the focus of research towards the development of numerical algorithms to model the three-dimensional propagation of hydraulic fractures in layered strata characterized by different mechanical properties and/or in situ stresses (Clifton and Abou-Sayed, 1981; Advani et al., 1990; Sousa et al., 1993; Shah et al., 1997; Peirce and Siebrits, 2001; Siebrits and Peirce, 2002). Devising an algorithm that can robustly and accurately model such a complicated process is by no means a simple task. Indeed, the algorithm has to cope with propagation of a fracture, fluid flow within the fracture and, in general, exchange of fluid between the fracture and the surrounding rock. In fact, a recent comparative study of many available hydraulic fracture simulators (Warpinski et al., 1993) shows significant differences between their predictions, with the fracture size varying by as much as a factor of three. The problem is compounded by the lack of exact solutions for a propagating penny-shaped hydraulic fracture to benchmark the numerical programs.

The first objective of this research is to construct rigorous solutions for the problem of a penny-shaped fluid-driven fracture, with a clear statement of their range of applicability. The other objective arises from a longstanding debate on the relevance of the rock toughness. This question is of fundamental importance for numerical modeling. If toughness is relevant, the shape of the fracture must be determined by tracking the fracture tip; if not, the fracture shape can be identified by the fluid front, which is much easier to follow than the fracture edge. There exist different points of view on this matter. For example, Geertsma and de Klerk (1969) argued that the toughness is irrelevant whenever the fracture is large enough, but Abé et al. (1976, 1979) came to the opposite conclusion from an analysis that distinguishes the fluid front from the crack edge.

An entirely different approach to the issue of toughness invokes an argument based on the ratio of the energy dissipated in the rock to create new fracture surfaces to the energy dissipated in the fluid by viscous flow (Detournay, 1999; Carbonell et al., 1999; Garagash, 2000). According to this argument, the influence of toughness can be neglected if this energy ratio is small. For a hydraulic fracture in plane strain, this criterion yields a critical value for a dimensionless toughness below which toughness is negligible (Carbonell et al., 1999). Interestingly, this criterion does not depend on the confining stress, in contrast to those proposed by Geertsma and de Klerk (1969) and Abé et al. (1976, 1979).

The energy argument suggests that there must be three regimes of the propagation: viscosity-dominated (in which the toughness may be neglected), toughness-dominated (in which the viscosity may be neglected), and transient (in which both parameters are important). The second objective of this research is to analyze the regimes of propagation of a penny-shaped hydraulic fracture in an impermeable elastic rock.

The structure of the paper is as follows. The problem formulation is described in Section 2. In Section 3, we discuss the scaling of the governing equations and we introduce the viscosity- and toughness-dominated regimes of fracture propagation. Sections 4 and 5 present asymptotic solutions for zero toughness and large toughness, respectively. The regimes of fracture propagation are analyzed in Section 6, and concluding remarks are given in Section 7.

2. Problem formulation

Consider an axisymmetric hydraulic fracture propagating in an infinite impermeable elastic medium characterized by Young's modulus E, Poisson's ratio v, and toughness K_{Ic} (see Fig. 1). An incompressible

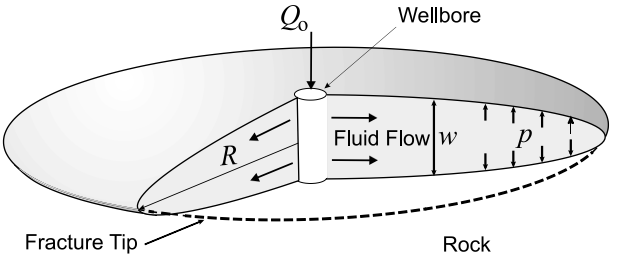

Fig. 1. A penny-shaped hydraulic fracture.

Newtonian fluid with viscosity μ is injected at the center of the fracture at constant volumetric rate Q_0. We seek to determine the crack aperture $w(r,t)$ as a function of the radial coordinate r and time t, the net pressure $p(r,t)$ (the difference between the fluid pressure p_f and the far-field compressive stress σ_0 perpendicular to the fracture plane), and the fracture radius $R(t)$.

Several assumptions are introduced to simplify this problem:

1. the fluid is injected from a point source (i.e., the wellbore radius is negligible compared to the fracture radius);
2. the fluid reaches the tip of the crack (i.e., the lag between the fracture tip and the fluid front is very small compared to the fracture radius);
3. the fracture propagates continuously in mobile equilibrium;
4. lubrication theory is applicable.

The legitimacy of Assumption 2 is based on an analysis of the near tip region of a fluid-driven fracture (Garagash and Detournay, 2000), which indicates that the lag λ reaches a maximum value $\lambda_0 \sim \mu V E'^2 \sigma_0^{-3}$ with V denoting the tip velocity, when $K_{Ic} = 0$. For typical values of the parameters, λ_0 is of the order of 10^{-1} m and thus generally very small compared to the fracture radius, which can reach dimension of order of 10^2 m. Furthermore, the actual lag λ could be very small compared to λ_0, if $K_{Ic} > 0$. By neglecting the lag, the solution does not depend on the far-field stress σ_0, which enters the formulation only as a reference stress.

The complete formulation of this problem relies on equations from elasticity and lubrication theories, on a fracture propagation criterion from linear elastic fracture mechanics, and on boundary conditions at the inlet and at the tip of the fracture.

The two coupled equations involving the fracture opening $w(r,t)$ and net pressure $p(r,t)$ consist of a non-local integral relation from elasticity (Sneddon, 1951)

$$w = \frac{8R}{\pi E'} \int_{r/R}^{1} \frac{\xi}{\sqrt{\xi^2 - (r/R)^2}} \int_0^1 \frac{x\, p(x\xi R, t)}{\sqrt{1-x^2}}\, \mathrm{d}x\, \mathrm{d}\xi \tag{1}$$

and a non-linear differential equation from lubrication theory (Batchelor, 1967)

$$\frac{\partial w}{\partial t} = \frac{1}{12\mu} \frac{1}{r} \frac{\partial}{\partial r} \left(r w^3 \frac{\partial p}{\partial r} \right) \tag{2}$$

Eq. (2), which is usually referred to as Reynolds equation, is obtained by eliminating the radial flow rate $q(r,t)$ between the fluid mass balance

$$\frac{\partial w}{\partial t} + \frac{1}{r} \frac{\partial}{\partial r} (rq) = 0 \tag{3}$$

and Poiseuille law

$$q = -\frac{w^3}{12\mu}\frac{\partial p}{\partial r} \tag{4}$$

In the above, E' is the plane strain modulus, which can be expressed in terms of E and v as $E' = E/(1-v^2)$.

According to linear elastic fracture mechanics (Kanninen and Popelar, 1985), the fracture propagation criterion takes the form

$$K_{\mathrm{I}} = K_{\mathrm{Ic}} \tag{5}$$

where K_{I} denotes the mode I stress intensity factor and K_{Ic} the material toughness. For a penny-shaped crack, K_{I} can be expressed as (Rice, 1968)

$$K_{\mathrm{I}} = \frac{2}{\sqrt{\pi R}}\int_0^R \frac{p(r,t)}{\sqrt{R^2-r^2}} r\,\mathrm{d}r \tag{6}$$

Condition (5) always applies, under Assumption 3 of continuous mobile equilibrium. The right-hand side of (6) is thus independent on time. The propagation condition (5) can equivalently be imposed as an asymptotic condition on the crack opening at the tip $r = R$ (Rice, 1968)

$$w \simeq 4\sqrt{\frac{2}{\pi}}\frac{K_{\mathrm{Ic}}}{E'}\sqrt{R-r}, \quad 1-\frac{r}{R} \ll 1 \tag{7}$$

The fracture tip is characterized by zero fracture opening

$$w = 0, \quad r = R \tag{8}$$

and a no-flow condition $q = 0$, which can be expressed in terms of opening and pressure by means of Poiseuille law (4) as

$$w^3\frac{\partial p}{\partial r} = 0, \quad r = R \tag{9}$$

Injection of fluid from the borehole is idealized by a source at the center of the fracture. Based on mass balance considerations, the source condition can be expressed as

$$2\pi \lim_{r\to 0} rq = Q_0 \tag{10}$$

It follows from (10) that $q \sim 1/r$ near the source. According to Poiseuille law (4), the fluid pressure is thus logarithmically singular at the source, $p \sim -\ln r$. The source can alternatively be taken into account by the global mass balance

$$Q_0 t = 2\pi\int_0^R wr\,\mathrm{d}r \tag{11}$$

This equation can also be obtained by integrating the local mass balance (3) and taking into account both boundary conditions (9) and (10).

The set consisting of the elasticity equation (1), Reynolds equation (2), the propagation criterion (5) or (7), the inlet condition (10) or (11) and the tip conditions (8) and (9) forms a complete system for determining $w(r,t)$, $p(r,t)$, and $R(t)$ with $0 \leqslant r \leqslant R(t)$, $t \geqslant t_0$, starting from known values of these quantities at an initial time t_0. However, in accordance with Assumptions 1 and 2, we are looking for solutions for which the influence of the initial conditions has vanished.

3. Scaling

3.1. General form

Scaling of this problem hinges on defining dimensionless crack opening Ω, net pressure Π, and fracture radius γ as

$$w(r,t) = \varepsilon(t)L(t)\Omega(\rho, \mathscr{P}(t)) \tag{12}$$

$$p(r,t) = \varepsilon(t)E'\Pi(\rho, \mathscr{P}(t)) \tag{13}$$

$$R(t) = L(t)\gamma(\mathscr{P}(t)) \tag{14}$$

With these definitions, we have introduced the dimensionless radial coordinate $\rho = r/R(t)$ $(0 \leqslant \rho \leqslant 1)$, a small number $\varepsilon(t)$, a length scale $L(t)$ of the same order of magnitude as the fracture radius $R(t)$, and a dimensionless parameter $\mathscr{P}(t)$, which depends monotonically on t. The form of the scaling (12)–(14) is motivated by elementary elasticity considerations, by noting that the average aperture scaled by the fracture radius is of the same order as the average net pressure scaled by the elastic modulus. Explicit forms of the parameters $\varepsilon(t)$, $L(t)$, and $\mathscr{P}(t)$ are given below for both the viscosity and the toughness scalings.

First, it is convenient to define a viscosity μ' and a toughness K', respectively proportional to μ and K_{Ic}, to avoid carrying numerical factors in the equations

$$\mu' = 12\mu, \quad K' = 4\left(\frac{2}{\pi}\right)^{1/2} K_{\mathrm{Ic}} \tag{15}$$

The main equations are transformed as follows, under the scaling (12)–(14).

- *Elasticity equation*

$$\Omega = \frac{8}{\pi}\gamma \int_\rho^1 \frac{\xi}{\sqrt{\xi^2 - \rho^2}} \int_0^1 \frac{x\Pi(x\xi)}{\sqrt{1-x^2}}\,\mathrm{d}x\,\mathrm{d}\xi \tag{16}$$

- *Lubrication equation.* The left-hand side $\partial w/\partial t$ of the lubrication equation (2) can now be written as

$$\frac{\partial w}{\partial t} = \left(\dot{\varepsilon}L + \varepsilon\dot{L}\right)\Omega - \varepsilon\dot{L}\rho\frac{\partial\Omega}{\partial\rho} + \varepsilon L\dot{\mathscr{P}}\left(\frac{\partial\Omega}{\partial\mathscr{P}} - \frac{\rho}{\gamma}\frac{\mathrm{d}\gamma}{\mathrm{d}\mathscr{P}}\frac{\partial\Omega}{\partial\rho}\right) \tag{17}$$

  while the right-hand side is transformed into

$$\frac{1}{\mu'}\frac{1}{r}\frac{\partial}{\partial r}\left(rw^3\frac{\partial p}{\partial r}\right) = \frac{\varepsilon^4 E' L}{\mu'\gamma^2}\frac{1}{\rho}\frac{\partial}{\partial r}\left(\rho\Omega^3\frac{\partial\Pi}{\partial\rho}\right) \tag{18}$$

  After multiplying both sides by $t/\varepsilon L$, we obtain a new form of the lubrication equation

$$\left(\frac{\dot{\varepsilon}t}{\varepsilon} + \frac{\dot{L}t}{L}\right)\Omega - \frac{\dot{L}t}{L}\rho\frac{\partial\Omega}{\partial\rho} + \dot{\mathscr{P}}t\left(\frac{\partial\Omega}{\partial\mathscr{P}} - \frac{\rho}{\gamma}\frac{\mathrm{d}\gamma}{\mathrm{d}\mathscr{P}}\frac{\partial\Omega}{\partial\rho}\right) = \frac{\varepsilon^3 E' t}{\mu'}\frac{1}{\gamma^2\rho}\frac{\partial}{\partial\rho}\left(\rho\Omega^3\frac{\partial\Pi}{\partial\rho}\right) \tag{19}$$

- *Global mass balance*

$$2\pi\varepsilon L^3\gamma^2\int_0^1 \Omega\rho\,\mathrm{d}\rho = Q_0 t \tag{20}$$

- *Propagation criterion.* The propagation criterion (5) can either be expressed in the form of the crack opening tip asymptote following (7)

$$\Omega = \frac{K'}{\varepsilon E' L^{1/2}} \gamma^{1/2} (1-\rho)^{1/2}, \quad 1-\rho \ll 1 \tag{21}$$

or as an integral constraint on the net pressure according to (6)

$$\frac{K'}{\varepsilon E' L^{1/2}} = \frac{2^{7/2}}{\pi} \gamma^{1/2} \int_0^1 \frac{\Pi}{\sqrt{1-\rho^2}} \rho \, \mathrm{d}\rho \tag{22}$$

3.2. Viscosity and toughness scalings

We now introduce viscosity and toughness scalings, respectively denoted by subscripts m and k. Although there is some freedom in defining the scaling parameters ε and L, the actual choice is restricted by the requirement that the dimensionless quantities (Ω, Π, and γ) should be O(1). Two equations are used to identify ε and L. The first equation expresses global mass conservation and the requirement that the average opening Ω is O(1)

$$\varepsilon L^3 = Q_0 t \tag{23}$$

The second equation depends on the particular scaling used. For the viscosity scaling, the dimensionless group containing the viscosity in the lubrication equation (19) is set to one

$$\frac{\mu'}{\varepsilon^3 E' t} = 1 \tag{24}$$

while for the toughness scaling, it is the dimensionless group with the toughness in the propagation criterion (21) or (22), which is set to one

$$\frac{K'}{\varepsilon E' L^{1/2}} = 1 \tag{25}$$

Note that in view of (23), (20) simplifies to yield a relationship between the dimensionless opening Ω and the radius γ

$$2\pi\gamma^2 \int_0^1 \Omega \rho \, \mathrm{d}\rho = 1 \tag{26}$$

Consider now the viscosity scaling. The small parameter ε_m and the lengthscale L_m are solution of (23) and (24)

$$\varepsilon_m = \left(\frac{\mu'}{E' t} \right)^{1/3}, \quad L_m = \left(\frac{E' Q_0^3 t^4}{\mu'} \right)^{1/9} \tag{27}$$

Since both ε_m and L_m are power laws of time, it follows that

$$\frac{\dot{\varepsilon}_m t}{\varepsilon_m} = -\frac{1}{3}, \quad \frac{\dot{L}_m t}{L_m} = \frac{4}{9} \tag{28}$$

It is also natural to introduce the dimensionless toughness $\mathscr{K}(t)$

$$\mathscr{K} = K' \left(\frac{t^2}{\mu'^5 Q_0^3 E'^{13}} \right)^{1/18} \tag{29}$$

so that the propagation criterion in terms of either the opening tip asymptote (21) or the integral pressure constraint (22) can be written as

$$\Omega_m = \mathscr{K}\gamma_m^{1/2}(1-\rho)^{1/2}, \quad 1-\rho \ll 1 \tag{30}$$

$$\mathscr{K} = \frac{2^{7/2}\gamma_m^{1/2}}{\pi}\int_0^1 \frac{\Pi_m}{\sqrt{1-\rho^2}}\rho\,\mathrm{d}\rho \tag{31}$$

In the viscosity scaling, the toughness $\mathscr{K}$ is the only parameter appearing in the set of the governing equations. Hence, $\mathscr{K}$ can be identified with $\mathscr{P}_m$ (the evolution parameter $\mathscr{P}$ for the viscosity scaling) and the solution in this scaling will be in the form $\Omega_m(\rho,\mathscr{K})$, $\Pi_m(\rho,\mathscr{K})$, and $\gamma_m(\mathscr{K})$. Note that $\mathscr{K}$ is a small number in the viscosity-dominated regime.

Next, we introduce the toughness scaling; ε_k and L_k are now determined from (23) and (25)

$$\varepsilon_k = \left(\frac{K'^6}{E'^6 Q_0 t}\right)^{1/5}, \quad L_k = \left(\frac{Q_0^2 E'^2 t^2}{K'^2}\right)^{1/5} \tag{32}$$

These expressions imply that

$$\frac{\dot{\varepsilon}_k t}{\varepsilon_k} = -\frac{1}{5}, \quad \frac{\dot{L}_k t}{L_k} = \frac{2}{5} \tag{33}$$

A dimensionless viscosity $\mathscr{M}(t)$ is logically defined as

$$\mathscr{M} = \mu'\left(\frac{Q_0^3 E'^{13}}{K'^{18} t^2}\right)^{1/5} \tag{34}$$

so that the lubrication equation (19) can be rewritten as

$$\mathscr{M}\left(\frac{1}{5}\Omega_k - \frac{2}{5}\rho\frac{\partial\Omega_k}{\partial\rho}\right) - \frac{2}{5}\mathscr{M}^2\left(\frac{\partial\Omega_k}{\partial\mathscr{M}} - \frac{\rho}{\gamma_k}\frac{\mathrm{d}\gamma_k}{\mathrm{d}\mathscr{M}}\frac{\partial\Omega_k}{\partial\rho}\right) = \frac{1}{\gamma_k^2\rho}\frac{\partial}{\partial\rho}\left(\rho\Omega_k^3\frac{\partial\Pi_k}{\partial\rho}\right) \tag{35}$$

In the above equation, we have already identified the viscosity $\mathscr{M}$ as the evolution parameter $\mathscr{P}_k$; hence, the solution in the toughness scaling will be in the form $\Omega_k(\rho,\mathscr{M})$, $\Pi_k(\rho,\mathscr{M})$, and $\gamma_k(\mathscr{M})$. The toughness-dominated regime corresponds to small values of the viscosity $\mathscr{M}$.

However, the dimensionless viscosity $\mathscr{M}$ and toughness $\mathscr{K}$ are simply related by

$$\mathscr{M} = \mathscr{K}^{-18/5} \tag{36}$$

The transition between viscosity- and toughness-dominated regimes can thus be understood in terms of only one parameter, which we select to be $\mathscr{K}$. Also, the small viscosity solution can equivalently be referred to as the large toughness solution. It is also interesting to note the relationships between the expressions for the small parameter ε and the lengthscale L in the two scalings

$$\frac{\varepsilon_m}{\varepsilon_k} = \mathscr{K}^{-6/5}, \quad \frac{L_m}{L_k} = \mathscr{K}^{2/5} \tag{37}$$

It then follows that the solution $\mathscr{F} = \{\Omega, \Pi, \gamma\}$ can be easily converted from one scaling to the other according to

$$\frac{\Omega_m}{\Omega_k} = \mathscr{K}^{4/5}, \quad \frac{\Pi_m}{\Pi_k} = \mathscr{K}^{6/5}, \quad \frac{\gamma_m}{\gamma_k} = \mathscr{K}^{-2/5} \tag{38}$$

The above analysis also indicates that, for the two limit cases $\mathscr{K} = 0$ and $\mathscr{K} = \infty$ ($\mathscr{M} = 0$), the solution is self-similar and thus does not depend on initial conditions. For any other value of $\mathscr{K}$, the solution is not self-similar and is a function of $\mathscr{K}$. In fact, since $\mathscr{K}$ is a monotonically increasing function of time, the solution necessarily evolves from the viscosity-dominated regime ($\mathscr{K} \ll 1$) towards the toughness-dominated regime

($\mathscr{K} \gg 1$). If $\mathscr{K}$ is the controlling parameter, the zero-toughness solution ($\mathscr{K} = 0$) provides the initial conditions from which the solution will evolve.

4. Zero-toughness solution

4.1. Problem formulation

We now turn towards the construction of the zero-toughness self-similar solution $\mathscr{F}_{m0} = \{\Omega_{m0}, \Pi_{m0}, \gamma_{m0}\}$ where

$$\Omega_{m0}(\rho) = \Omega_m(\rho, 0), \quad \Pi_{m0}(\rho) = \Pi_m(\rho, 0), \quad \gamma_{m0} = \gamma_m(0)$$

It is actually convenient to rescale the opening according to

$$\overline{\Omega}_{m0}(\rho) = \frac{\Omega_{m0}(\rho)}{\gamma_{m0}} \tag{39}$$

which allows, as shown below, to first solve for $\overline{\mathscr{F}}_{m0} = \{\overline{\Omega}_{m0}, \Pi_{m0}\}$ and then compute γ_{m0}. Following Barr (1991), it is also advantageous to rewrite the conventional elasticity equation (1) by reducing its right-hand side to a single integral (see Appendix A for details)

$$w(r,t) = \frac{8R}{\pi E'} \int_0^1 G(r/R, \xi) p(\xi R, t) \xi \, \mathrm{d}\xi \tag{40}$$

where the kernel G is given in closed form as

$$G(\rho, \xi) = \begin{cases} \dfrac{1}{\rho} F\left(\arcsin \sqrt{\dfrac{1-\rho^2}{1-\xi^2}}, \dfrac{\xi^2}{\rho^2} \right), & \rho > \xi \\ \dfrac{1}{\xi} F\left(\arcsin \sqrt{\dfrac{1-\xi^2}{1-\rho^2}}, \dfrac{\rho^2}{\xi^2} \right), & \rho < \xi \end{cases} \tag{41}$$

with F denoting the incomplete elliptic integral of the first kind (Abramowitz and Stegun, 1964).

Thus the system of equations for the limit case $\mathscr{K} = 0$ can be written in terms of $\overline{\Omega}_{m0}(\rho)$ and $\Pi_{m0}(\rho)$ as follows:

- *Elasticity equation:*

$$\overline{\Omega}_{m0} = \frac{8}{\pi} \int_0^1 G(\rho, \xi) \Pi_{m0}(\xi) \xi \, \mathrm{d}\xi \tag{42}$$

  with the kernel G given by (41).
- *Lubrication equation:*

$$\int_\rho^1 \overline{\Omega}_{m0} \xi \, \mathrm{d}\xi + \frac{4}{9} \rho^2 \overline{\Omega}_{m0} = -\rho \overline{\Omega}_{m0}^3 \frac{\mathrm{d}\Pi_{m0}}{\mathrm{d}\rho} \tag{43}$$

  This form of the lubrication equation is obtained by integrating the lubrication equation (19) from ρ to 1 with the weight ξ and making use of the tip conditions (45).
- *Propagation criterion:*

$$\int_0^1 \frac{\Pi_{m0}}{\sqrt{1-\rho^2}} \rho \, \mathrm{d}\rho = 0 \tag{44}$$

- *Conditions at the tip* ($\rho = 1$)*:*

$$\overline{\Omega}_{m0} = 0, \quad \overline{\Omega}_{m0}^3 \frac{\mathrm{d}\Pi_{m0}}{\mathrm{d}\rho} = 0 \tag{45}$$

- *Global mass balance:*

$$\gamma_{m0} = \left(2\pi \int_0^1 \overline{\Omega}_{m0} \rho \, \mathrm{d}\rho\right)^{-1/3} \tag{46}$$

The first four equations (42)–(45) are complete with respect to $\overline{\Omega}_{m0}(\rho)$ and $\Pi_{m0}(\rho)$. The dimensionless radius γ_{m0} can be computed from (46) once the function $\overline{\Omega}_{m0}(\rho)$ has been identified; this justifies the rescaling $\gamma_{m0}\overline{\Omega}_{m0} = \Omega_{m0}$.

4.2. Tip and inlet asymptotic behavior

The assumption that the fluid front coincides with the crack tip results in a pressure singularity at the tip. This singularity must be properly accounted for in order to obtain an accurate solution of the problem. It was first shown by Spence and Sharp (1985) that the opening behaves near the tip as $(R-r)^{2/3}$ and the net pressure as $(R-r)^{-1/3}$, under the assumptions of zero lag ($\lambda = 0$) and zero toughness ($K' = 0$). These asymptotes were also found as an exact solution to the problem of a semi-infinite hydraulic fracture propagating in an impermeable rock with $\lambda = 0$ and $K' = 0$ (Desroches et al., 1994). For a Newtonian fluid, the tip asymptotes for the crack opening w and the net pressure p are

$$w = 2^{1/3} \times 3^{5/6} \left(\frac{\mu' \dot{R} R^2}{E'}\right)^{1/3} \hat{\xi}^{2/3} + \mathrm{O}(\hat{\xi}^{5/3}), \quad p = -\frac{1}{6^{2/3}} \left(\frac{\mu' \dot{R} E'^2}{R}\right)^{1/3} \hat{\xi}^{-1/3} + \mathrm{O}(\hat{\xi}^{2/3}) \tag{47}$$

where $\hat{\xi} = 1 - r/R \ll 1$. Thus, the pressure is singular both at the inlet and at the tip. In dimensionless form, these asymptotes are rewritten as follows.

- *Inlet asymptote*. The pressure is logarithmically singular at the source

$$\Pi_{m0} \sim -\ln \rho, \quad \rho \ll 1 \tag{48}$$

- *Tip asymptote*. The tip asymptotes for $\overline{\Omega}_{m0}$ and Π_{m0} are deduced by rescaling the singular solution (47) in terms of $\overline{\Omega}_{m0}$, Π_{m0}, and ρ

$$\overline{\Omega}_{m0} \simeq 2 \times 3^{1/6}(1-\rho)^{2/3}, \quad \Pi_{m0} \simeq -3^{-4/3}(1-\rho)^{-1/3}, \quad 1-\rho \ll 1 \tag{49}$$

It is interesting to note that the rewriting of the asymptotes (47) in terms of $\overline{\Omega}_{m0}$ is only possible because of the rescaling (39).

4.3. Method of solution

The method for constructing a solution of the formulated problem is inspired by, although different from, the scheme described by Spence and Sharp (1985) and the approach used by Carbonell et al. (1999) to find the zero-toughness solution for a plane strain fracture.

The solution is sought in terms of series expansions. Since the non-linearity of this problem is only introduced by the lubrication equation, the superposition principle can be applied to solve the elasticity equation, taking also into account the boundary conditions and the propagation criterion. Here, the

solution is sought as a sum of a general solution $\overline{\mathscr{F}}^{*} = \{\overline{\Omega}^{*}, \Pi^{*}\}$ having the expected behavior (49) at the fracture tip, and a particular solution $\overline{\mathscr{F}}^{**} = \{\overline{\Omega}^{**}, \Pi^{**}\}$ having the correct singularity (48) at the source

$$\overline{\mathscr{F}}_{m0} = \overline{\mathscr{F}}^{*}(\rho) + B\overline{\mathscr{F}}^{**}(\rho) \tag{50}$$

where B is an as yet unknown coefficient. Furthermore, the general solution is represented in terms of infinite series of base functions $\Pi_i^{*}(\rho)$ and $\overline{\Omega}_i^{*}(\rho)$

$$\Pi_{m0} = \sum_{i=1}^{\infty} A_i \Pi_i^{*}(\rho) + B\,\Pi^{**}(\rho) \tag{51}$$

$$\overline{\Omega}_{m0} = \sum_{i=1}^{\infty} C_i \overline{\Omega}_i^{*}(\rho) + B\overline{\Omega}^{**}(\rho) \tag{52}$$

where A_i and C_i are also unknown coefficients.

Both the general solution $\overline{\mathscr{F}}^{*}$ and the particular solution $\overline{\mathscr{F}}^{**}$ have to satisfy the elasticity equation (42). A novelty of the approach described here is that application of (42) differs for $\overline{\mathscr{F}}^{*}$ and $\overline{\mathscr{F}}^{**}$. While $\overline{\Omega}^{**}$ and Π^{**} *exactly* satisfy the elasticity equation (42), the pressure and opening base functions $\overline{\Omega}_i^{*}$ and Π_i^{*} are chosen independently. Instead, the elasticity equation (42) provides a relationship between the coefficients of the series for opening and for pressure, $\{A_i\}$ and $\{C_i\}$. Further, an approximate solution $\overline{\mathscr{F}}^{*(n_\Pi, n_\Omega)}$ is sought by considering the first n_Π and n_Ω terms of the series expansions (51) and (52) for the pressure and opening, respectively.

4.4. Particular solution

A particular solution of the form $\Pi^{**} = -\ln\rho + D$ satisfies the inlet asymptotic behavior, and allows an easy determination of the constant D from the zero-toughness condition (44). Thus,

$$\Pi^{**} = -\ln\rho + \ln 2 - 1 \tag{53}$$

Substituting the above expression into the elasticity equation (42) yields the corresponding opening $\overline{\Omega}^{**}(\rho)$

$$\overline{\Omega}^{**} = \frac{8}{\pi}(1-\rho^2)^{1/2} - \frac{8}{\pi}\rho\arccos\rho \tag{54}$$

Since the pressure $\Pi^{**}(\rho)$ satisfies the zero-toughness condition and is finite at the tip, $\overline{\Omega}^{**}(\rho)$ must behave as $(1-\rho)^{3/2}$ near $\rho = 1$. Indeed, the asymptotic expansion of (54) near the tip yields

$$\overline{\Omega}^{**}(\rho) = \frac{2^{9/2}}{3\pi}(1-\rho)^{3/2} + \mathrm{O}[(1-\rho)^{5/2}], \quad 1-\rho \ll 1 \tag{55}$$

4.5. General solution

The central part of this approach is the construction of the general solution $\overline{\mathscr{F}}^{*}(\rho)$. The set of base functions, which must have the appropriate behavior at the tip according to (47), is chosen to be orthogonal. Such functions are Jacobi polynomials multiplied by the proper weights

$$\Pi_i^{*}(\rho) = -\overline{\Pi}_i^{*}(\rho) + \omega_i \tag{56}$$

$$\overline{\Pi}_i^{*}(\rho) = \frac{(1-\rho)^{-1/3}}{h_{i-1}^{1/2}\left(\frac{4}{3},2\right)} G_{i-1}\left(\frac{4}{3},2,\rho\right) \tag{57}$$

$$\overline{\Omega}_i^*(\rho) = \frac{(1-\rho)^{2/3}}{h_{i-1}^{1/2}\left(\frac{10}{3},2\right)} G_{i-1}\left(\frac{10}{3},2,\rho\right) \tag{58}$$

In the above, $G_i(p,q,\rho)$ is the Jacobi polynomial of order i defined on the interval $[0,1]$

$$G_i(p,q,\rho) = \frac{\Gamma(q+i)}{\Gamma(p+2i)} \sum_{j=0}^{i} (-1)^j \binom{i}{j} \frac{\Gamma(p+2i-j)}{\Gamma(q+i-j)} \rho^{i-j} \tag{59}$$

and $h_i(p,q)$ is the norm of G_i defined as (Abramowitz and Stegun, 1964)

$$\int_0^1 (1-\rho)^{p-q} \rho^{q-1} G_i(p,q,\rho) G_j(p,q,\rho)\, \mathrm{d}\rho = h_i(p,q)\delta_{ij} \tag{60}$$

where δ_{ij} is the Kronecker symbol. Hence,

$$h_i(p,q) = \frac{i!\Gamma(i+q)\Gamma(i+p)\Gamma(i+p-q+1)}{(2i+p)\Gamma^2(2i+p)} \tag{61}$$

It can be easily shown that $\{\overline{\Omega}_i^*(\rho)\}$ and $\{\overline{\Pi}_i^*(\rho)\}$ are orthonormal sets of functions in the following sense [1]

$$\int_0^1 \overline{\Omega}_i^*(\rho)\overline{\Omega}_j^*(\rho)\rho\, \mathrm{d}\rho = \delta_{ij} \tag{62}$$

$$\int_0^1 \overline{\Pi}_i^*(\rho)\overline{\Pi}_j^*(\rho)\rho\, \mathrm{d}\rho = \delta_{ij} \tag{63}$$

The constants ω_i in (56) are adjustments to the pressure base functions such that each one fulfills the constraint (44). They are thus determined from

$$\omega_i = \int_0^1 \frac{\overline{\Pi}_i^*(\rho)}{\sqrt{1-\rho^2}} \rho\, \mathrm{d}\rho \tag{64}$$

Table 1 lists the coefficients ω_i for $i = 1,\ldots,4$.

Substituting the finite series for Π^* and $\overline{\Omega}^*$ into the elasticity equation (42) eventually yields the relationship between the two sets of coefficients

$$C_i^{(n_\Omega,n_\Pi)} = \sum_{j=1}^{n_\Pi} L_{ij} A_j^{(n_\Omega,n_\Pi)} \tag{65}$$

where

$$L_{ij} = \frac{8}{\pi} \int_0^1 \overline{\Omega}_i^*(\rho) \left[\int_0^1 G(\rho,\xi)\Pi_j^*(\xi)\xi\, \mathrm{d}\xi \right] \rho\, \mathrm{d}\rho \tag{66}$$

Appendix B provides some details for the accurate evaluation of the elements L_{ij}, in view of the weak singularity of the kernel G. Note that the L_{ij} have to be calculated only once, as they do not depend on the parameters n_Ω and n_Π. Numerical results indicate that for the given ith mode of pressure, the first $(i+1)$ terms of the opening series provide a fairly good approximation of the corresponding integral. Thus, we can set $n_\Omega = n_\Pi + 1 = n + 1$. The computed coefficients L_{ij} are listed in Table 2 for $n = 4$.

[1] Note that functions Π_i^* are not orthogonal. It has been verified that orthogonalization of this set of functions does not improve the convergence and the accuracy of the solution.

Table 1
Values of constants ω_i for $i = 1, \ldots, 4$

ω_1	ω_2	ω_3	ω_4
2.479	0.7615	0.6329	0.5275

Table 2
Coefficients L_{ij} for $n = 4$

L_{ij}	1	2	3	4
1	1.912	2.546	0.8201	0.6290
2	0.1982	−0.03698	0.8135	0.1219
3	0.003556	−0.08572	−0.04883	0.4586
4	0.003472	−0.007786	−0.08325	−0.02817
5	0.0009090	−0.005216	−0.006443	−0.07449

4.6. Lubrication equation

The coefficients $A_i^{(n)}$ and $B^{(n)}$ are finally determined from the lubrication equation by means of the least squares method. The truncated series of base functions for the opening and the pressure are substituted into the lubrication equation (43). Then, the left and right hand sides of the equation are computed at a set of m equally spaced control points ($m = 10$ for $n = 1, \ldots, 4$). Now, we can construct a cost function as a sum of squares of discrepancies at the control points

$$\Delta(A_1^{(n)}, \ldots, A_n^{(n)}, B^{(n)}) = \sum_{i=1}^{m} \left[\frac{\Xi^r(\rho_i; A_1^{(n)}, \ldots, A_n^{(n)}, B^{(n)})}{\Xi^l(\rho_i; A_1^{(n)}, \ldots, A_n^{(n)}, B^{(n)})} - 1 \right]^2 \tag{67}$$

where $\rho_1 = 0$ and $\rho_m = 1$. The expressions for the left and right hand sides of the lubrication equation Ξ^l and Ξ^r, respectively, are given in Appendix C.

The unknown coefficients $A_i^{(n)}$ and $B^{(n)}$ are to be computed by minimizing the cost function Δ. The procedure starts from $n = 1$. Then, the solution from the current n is used as an initial guess for the next value $n = n + 1$. It is interesting to note that the dependence of the coefficients $A_i^{(n)}$ and $B^{(n)}$ upon n stems only from the non-linearity of the lubrication equation.

4.7. Results

The coefficients $B^{(n)}$, $A_i^{(n)}$, and $C_i^{(n)}$ are listed in Table 3 for $n = 1, \ldots, 4$, while the opening $\overline{\Omega}_{m0}^{(n)}(0)$ at the fracture inlet and the constant $\gamma_{m0}^{(n)}$ are given in Table 4, also for $n = 1, \ldots, 4$. The opening $\overline{\Omega}_{m0}^{(n)}$ and net pressure $\Pi_{m0}^{(n)}$ are plotted in Fig. 2 for $n = 4$. (The pressure plot is truncated at both ends because of the singularity at the tip and at the source.) However, the first-order solution $n = 1$ is already an excellent approximation, as it could hardly be distinguished from the solution $n = 4$ if it were plotted in Fig. 2. This can be also confirmed by examining the convergence of the solution in Table 4. These results show the robustness of the calculation scheme and the very rapid convergence of the solution with n. The explicit expressions for the opening estimate $\overline{\Omega}_{m0}^{(1)}(\rho)$ and the net pressure estimate $\Pi_{m0}^{(1)}(\rho)$ are given below

$$\overline{\Omega}_{m0}^{(1)} = \left[\frac{\sqrt{70}}{3} C_1^{(1)} + \frac{4\sqrt{5}}{9} C_2^{(1)} (13\rho - 6) \right] (1-\rho)^{2/3} + B^{(1)} \left[\frac{8}{\pi} (1-\rho)^{1/2} - \frac{8}{\pi} \rho \arccos \rho \right] \tag{68}$$

$$\Pi_{m0}^{(1)} = A_1^{(1)} \left[\omega_1 - \frac{2}{3(1-\rho)^{1/3}} \right] - B^{(1)} \left(\ln \frac{\rho}{2} + 1 \right) \tag{69}$$

Table 3
Coefficients $B^{(n)}$, $A_i^{(n)}$, and $C_i^{(n)}$ for $n = 1, \ldots, 4$

n	1	2	3	4
$B^{(n)} \times 10^2$	9.269	9.011	9.389	9.320
$A_1^{(n)} \times 10^1$	3.581	3.499	3.409	3.386
$A_2^{(n)} \times 10^3$	–	5.442	9.805	11.33
$A_3^{(n)} \times 10^3$	–	–	2.130	2.358
$A_4^{(n)} \times 10^4$	–	–	–	1.646
$C_1^{(n)} \times 10^1$	6.846	6.828	6.784	6.783
$C_2^{(n)} \times 10^2$	7.098	6.916	6.894	6.864
$C_3^{(n)} \times 10^4$	–	7.777	2.676	1.930
$C_4^{(n)} \times 10^4$	–	–	9.299	8.867
$C_5^{(n)} \times 10^4$	–	–	–	2.212

Table 4
Opening at the source $\overline{\Omega}_{m0}^{(n)}(0)$ and radius $\gamma_{m0}^{(n)}$ for $n = 1, \ldots, 4$

n	$\overline{\Omega}_{m0}^{(n)}(0)$	$\gamma_{m0}^{(n)}$
1	1.722	6.955×10^{-1}
2	1.729	6.965×10^{-1}
3	1.710	6.974×10^{-1}
4	1.713	6.976×10^{-1}

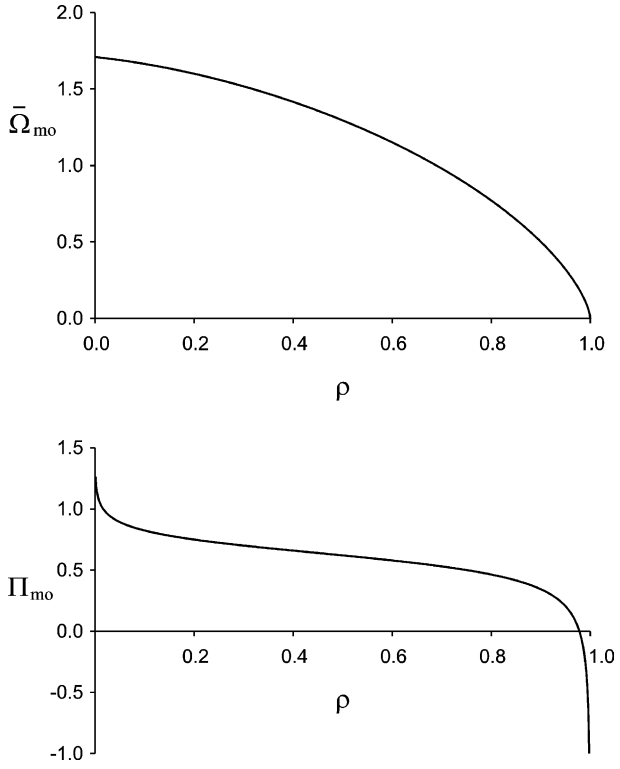

Fig. 2. Crack opening $\overline{\Omega}_{m0}^{(n)}$ and net pressure $\Pi_{m0}^{(n)}(\rho)$ for $n = 4$.

The very small number of terms in the expansions that are needed to capture the solution accurately is largely due to the proper account of the singular behavior of the solution at the source and at the tip.

5. Large-toughness asymptotic solution

5.1. Problem formulation

The large toughness solution corresponds to the situation when the dimensionless viscosity $\mathscr{M} \ll 1$. The toughness scaling is appropriate for this case. The system of equations for the toughness-dominated regime can be rewritten in terms of Π_k, Ω_k, and γ_k as follows:

- *Elasticity equation:*

$$\Omega_k = \frac{8\gamma_k}{\pi} \int_\rho^1 \frac{\xi}{\sqrt{\xi^2 - \rho^2}} \int_0^1 \frac{x\Pi_k(x\xi, t)}{\sqrt{1 - x^2}} \, \mathrm{d}x \, \mathrm{d}\xi \tag{70}$$

- *Lubrication equation:*

$$\mathscr{M}\left(\int_\rho^1 \Omega_k \xi \, \mathrm{d}\xi + \frac{2}{5}\rho^2 \Omega_k \right) + \mathrm{O}(\mathscr{M}^2) = -\frac{\rho}{\gamma_k^2} \Omega_k^3 \frac{\partial \Pi_k}{\partial \rho} \tag{71}$$

which is deduced from the lubrication equation (35), after integrating both sides of the equation from ρ to 1 with the weight ξ. Also, the term $\mathrm{O}(\mathscr{M}^2)$ in the left-hand side of (71) has not be written explicitly, as we only seek to determine the solution to order of $\mathscr{M}$.

- *Propagation criterion:*

$$\gamma_k^{-1/2} = \frac{8\sqrt{2}}{\pi} \int_0^1 \frac{\Pi_k}{\sqrt{1 - \rho^2}} \rho \, \mathrm{d}\rho \tag{72}$$

- *Global mass balance:*

$$2\pi\gamma_k^2 \int_0^1 \Omega_k \rho \, \mathrm{d}\rho = 1 \tag{73}$$

Note that the pressure near the tip is now logarithmically singular. This result can be directly verified by substituting the square-root opening asymptote (7) in the Poiseuille equation (4).

5.2. First-order asymptotic solution

We now seek a solution $\mathscr{F}_k = \{\Omega_k, \Pi_k, \gamma_k\}$ of the system of equations (70)–(73) to order of $\mathscr{M}$ in the form of a *regular* asymptotic expansion, following the approach used by Garagash (2000) for the equivalent plane strain problem

$$\mathscr{F}_k(\mathscr{M}) = \mathscr{F}_{k0} + \mathscr{M}\mathscr{F}_{k1} + \mathrm{O}(\mathscr{M}^2) \tag{74}$$

where $\mathscr{F}_{k0} = \{\Omega_{k0}, \Pi_{k0}, \gamma_{k0}\}$ and $\mathscr{F}_{k1} = \{\Omega_{k1}, \Pi_{k1}, \gamma_{k1}\}$. Substituting the expansions (74) into (70)–(73) and collecting terms $\mathrm{O}(1)$ and $\mathrm{O}(\mathscr{M})$ results in the following sets of equations for the zero- and first-order terms in the expansions (74).

- $O(\mathscr{M}^0)$:

$$\Omega_{k0} = \frac{8\gamma_{k0}}{\pi} \int_\rho^1 \frac{\xi}{\sqrt{\xi^2 - \rho^2}} \int_0^1 \frac{x\Pi_{k0}(x\xi)}{\sqrt{1-x^2}}\, \mathrm{d}x\, \mathrm{d}\xi \tag{75}$$

$$\frac{\mathrm{d}\Pi_{k0}}{\mathrm{d}\rho} = 0 \tag{76}$$

$$\gamma_{k0}^{-1/2} = \frac{8\sqrt{2}}{\pi} \int_0^1 \frac{\Pi_{k0}}{\sqrt{1-\rho^2}}\, \rho\, \mathrm{d}\rho \tag{77}$$

$$\gamma_{k0} = \omega_{k0}^{-1/2} \tag{78}$$

- $O(\mathscr{M}^1)$:

$$\Omega_{k1} = \frac{8\gamma_{k1}}{\pi} \int_\rho^1 \frac{\xi}{\sqrt{\xi^2 - \rho^2}} \int_0^1 \frac{x\Pi_{k0}(x\xi)}{\sqrt{1-x^2}}\, \mathrm{d}x\, \mathrm{d}\xi + \frac{8\gamma_{k0}}{\pi} \int_\rho^1 \frac{\xi}{\sqrt{\xi^2 - \rho^2}} \int_0^1 \frac{x\Pi_{k1}(x\xi)}{\sqrt{1-x^2}}\, \mathrm{d}x\, \mathrm{d}\xi \tag{79}$$

$$\int_\rho^1 \Omega_{k0}\xi\, \mathrm{d}\xi + \frac{2}{5}\rho^2\Omega_{k0} = -\frac{\rho}{\gamma_{k0}^2}\Omega_{k0}^3 \frac{\mathrm{d}\Pi_{k1}}{\mathrm{d}\rho} \tag{80}$$

$$\gamma_{k1} = -\frac{16\sqrt{2}}{\pi}\gamma_{k0}^{3/2} \int_0^1 \frac{\Pi_{k1}}{\sqrt{1-\rho^2}}\, \rho\, \mathrm{d}\rho \tag{81}$$

$$\gamma_{k1} = -\frac{1}{2}\omega_{k1}\gamma_{k0}^3 \tag{82}$$

where

$$\omega_{ki} = 2\pi \int_0^1 \Omega_{ki}\rho\, \mathrm{d}\rho \tag{83}$$

The zero-order solution $\mathscr{F}_{k0}$ corresponds to an inviscid fluid ($\mathscr{M} = 0$). As expected, (76) implies that the pressure is spatially uniform. The solution $\mathscr{F}_{k0}$ is given in closed form by

$$\Pi_{k0} = \frac{\pi}{8}\left(\frac{\pi}{12}\right)^{1/5} \simeq 0.3004 \tag{84}$$

$$\Omega_{k0} = \left(\frac{3}{8\pi}\right)^{1/5} (1-\rho^2)^{1/2} \tag{85}$$

$$\gamma_{k0} = \left(\frac{3}{\pi\sqrt{2}}\right)^{2/5} \simeq 0.8546 \tag{86}$$

Consider next the first-order term $\mathscr{F}_{k1}$. Substituting Ω_{k0} and γ_{k0} into (80) yields a simple equation for $\Pi_{k1}(\rho)$

$$\frac{\mathrm{d}\Pi_{k1}}{\mathrm{d}\rho} = -A_k\left(\frac{1}{3\rho} + \frac{2}{5}\frac{\rho}{1-\rho^2}\right) \tag{87}$$

which can be integrated to give an explicit expression for $\Pi_{k1}(\rho)$ up to an unknown constant Π^*_{k1}

$$\Pi_{k1} = \Pi^*_{k1} - A_k\left[\frac{1}{3}\ln\rho - \frac{1}{5}\ln(1-\rho^2)\right] \tag{88}$$

with

$$A_k = \left(\frac{\pi}{8\Pi_{k0}}\right)^2 \simeq 1.709$$

Substituting Π_{k0} and Π_{k1} into (79) yields $\Omega_{k1}(\rho)$ (see Appendix D for details)

$$\Omega_{k1} = B_k\left(1-\rho^2\right)^{1/2} - \frac{8}{3\pi}A_k\gamma_{k0}\left[\left(\ln 2 - \frac{4}{5}\right)(1-\rho^2)^{1/2} + \rho\arccos\rho - \frac{6}{5}I^*(\rho)\right] \tag{89}$$

with

$$B_k = \frac{8}{\pi}(\gamma_{k1}\Pi_{k0} + \gamma_{k0}\Pi^*_{k1})$$

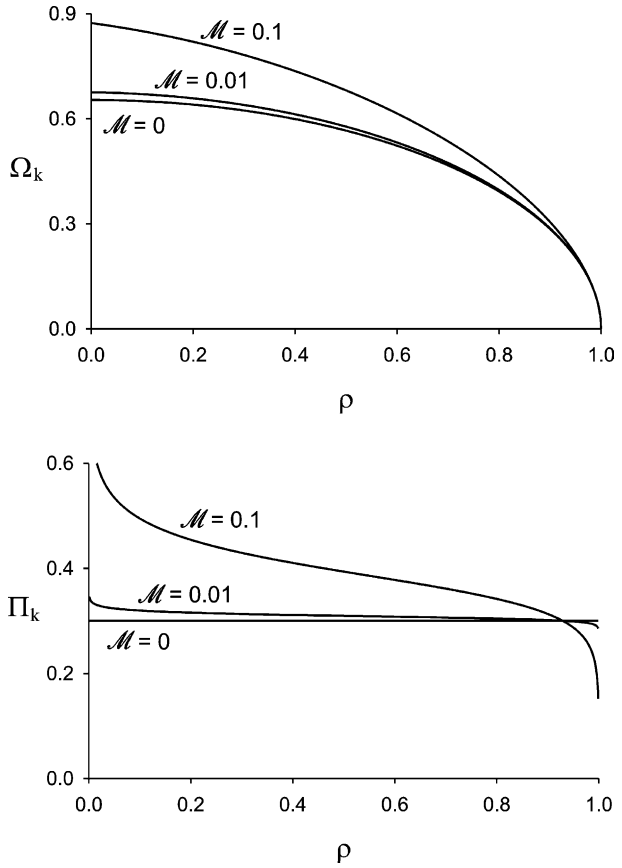

Fig. 3. Crack opening and net pressure in the toughness-dominated regime.

The function $I^*(\rho)$ defined as

$$I^*(\rho) = \int_\rho^1 \sqrt{\frac{1-\xi^2}{\xi^2-\rho^2}} \arcsin \xi \, \mathrm{d}\xi \tag{90}$$

has to be evaluated numerically. Although the opening is not known in closed form, the corresponding volume ω_{k1} can nonetheless be integrated analytically (see Appendix D for details)

$$\omega_{k1} = \frac{2\pi}{3} B_k - \frac{16}{9} A_k \gamma_{k0} \left(\ln 2 - \frac{14}{15} \right) \tag{91}$$

The two unknowns Π^*_{k1} and γ_{k1} are finally determined by solving (81) and (82)

$$\gamma_{k1} = -\frac{544}{75\pi^2} \simeq -0.7349 \tag{92}$$

$$\Pi^*_{k1} = \frac{2^{4/5}(32 + 75 \ln 2)}{75 \times 3^{3/5} \pi^{2/5}} \simeq 0.6380 \tag{93}$$

It then follows that

$$B_k \simeq 0.8264$$

5.3. Results

Fig. 3 shows the solution for different values of $\mathscr{M}$. An interesting result pertains to the singular nature of the first-order pressure solution (88) near the tip and the inlet. The logarithmic singularity near the tip results from neglecting the fluid lag, while the logarithmic singularity near the inlet is caused by neglecting the wellbore radius. The zero-order solution does not capture these singularities.

6. Regimes of fracture propagation

The solution for a penny-shaped hydraulic fracture depends only on one parameter, which we select to be the toughness $\mathscr{K}$. In principle, we can define three regimes of propagation:

- viscosity-dominated regime ($\mathscr{K} < \mathscr{K}_{m0}$), where the solution $\mathscr{F}$ can be approximated by $\mathscr{F}_{m0}$ (the zero-toughness solution);
- mixed-regime ($\mathscr{K}_{m0} < \mathscr{K} < \mathscr{K}_{k0}$), where the solution depends on both the viscosity and the toughness;
- toughness-dominated regime ($\mathscr{K} > \mathscr{K}_{k0}$), where the solution $\mathscr{F}$ can be approximated by the $\mathscr{F}_{k0}$ (the zero-viscosity solution).

Strictly speaking, the viscosity- and toughness-dominated regimes of propagation correspond to $\mathscr{K} \ll 1$ and $\mathscr{K} \gg 1$, respectively. It is possible, however, to identify the bounds $\mathscr{K}_{m0}$ and $\mathscr{K}_{k0}$, such that $\mathscr{K} < \mathscr{K}_{m0}$ corresponds for all practical purposes to the viscosity-dominated regime, and $\mathscr{K} > \mathscr{K}_{k0}$ to the toughness-dominated regime. Pragmatically, these bounds can be assessed by considering the dependence of the fracture radius γ_m on $\mathscr{K}$.

Consider first the large toughness asymptotic solution (74) in terms of γ in the viscosity scaling. Using the equivalence (36) and (38) between the two scalings, we can express γ_m for large $\mathscr{K}$ as

$$\gamma_m \simeq \gamma_{k0} \mathscr{K}^{-2/5} + \gamma_{k1} \mathscr{K}^{-4}, \quad \text{for } \mathscr{K} \gg 1 \tag{94}$$

It can be readily deduced from (94) that the error of approximating γ_m by the zero-viscosity solution $\gamma_{m\infty} = \gamma_{k0} \mathscr{K}^{-2/5}$ is less than 1% for $\mathscr{K} = 3.5$; thus, it is appropriate to adopt $\mathscr{K}_{k0} \simeq 3.5$.

Identification of the practical upper bound $\mathscr{K}_m$ of the viscosity-dominated regime requires to compare the zero-toughness solution with a general numerical solution. Such an approach has been successfully applied to the analysis of the plane strain problem (Carbonell et al., 1999; Garagash, 2000). However, unlike for the plane strain case, the solution for a penny-shaped fracture is not self-similar in all the regimes of propagation. Thus, the radial hydraulic fracture solution must, in general, be computed numerically by solving an evolution problem, while in the plane strain case, self-similar solutions depending on a parameter similar to $\mathscr{K}$ (but which does not depend on time) can be computed independently in the form of series expansions (Spence and Sharp, 1985).

Table 5
Parameters for tests I and II

Quantity	Test I	Test II
Q (m^3/s)	0.053	3×10^{-5}
σ_0 (MPa)	41.4	6.86
E (GPa)	38.8	5
ν	0.15	0.42
μ (MPa s)	2×10^{-8}, 8×10^{-8}	10^{-9}
r_0 (m)	0.079	0.079
K_{Ic} (MPa $m^{1/2}$)	1	0.129, 0.194, 0.244, 0.322, 0.387, 0.463, 1.27

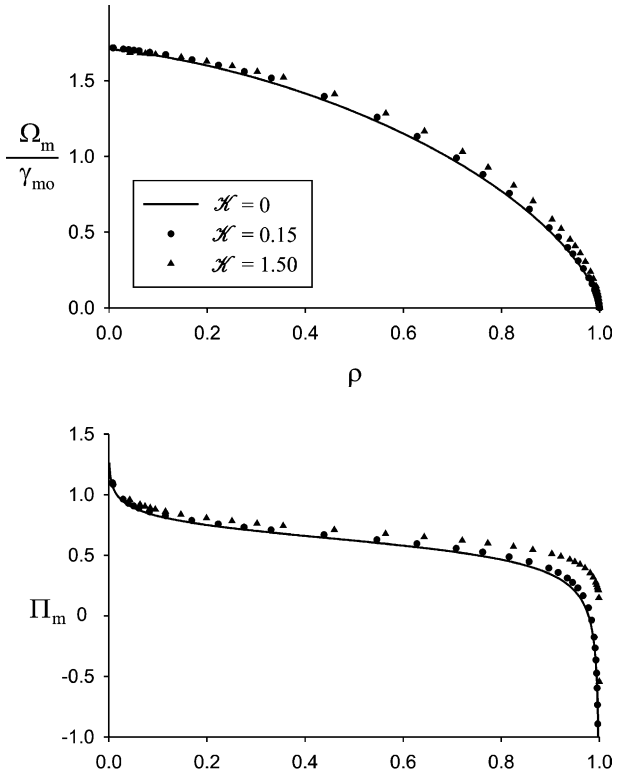

Fig. 4. Comparison of the opening and pressure of analytical solution and Loramec simulation given in the viscosity scaling for $\mathscr{K} = 0.15$ and 1.5.

Further analysis is based on the numerical results obtained with the code Loramec (Desroches, 2000). This code is designed to simulate the propagation of a plane strain and a penny-shaped hydraulic fractures. The algorithm is based on a combination of the finite difference and boundary element methods and is made efficient through the use of a moving mesh. A description of Loramec can be found elsewhere (Desroches and Thiercelin, 1993; Carbonell et al., 1999). We only note here that both the well radius and the fluid lag are accounted for explicitly in Loramec.

Since Loramec is formulated in terms of dimensional variables, two sets of parameters are considered (see Table 5). The parameters for Test I are similar to field parameters, while those for Test II correspond to laboratory experiments. All results are further given in dimensionless form; they are computed from the numerical solution at various stages of propagation of the fracture.

First, we compare numerical results corresponding to small and large values of the dimensionless toughness to the asymptotic solutions derived earlier. Fig. 4 shows the opening and the pressure in the viscosity scaling for small values of $\mathscr{K}$. It is clear that while the parameter $\mathscr{K}$ is small the matching between the two solutions is very good. However, as this parameter increases the difference between the asymptotic and numerical solutions becomes more and more evident. A similar situation is observed for large values of toughness (see Fig. 5).

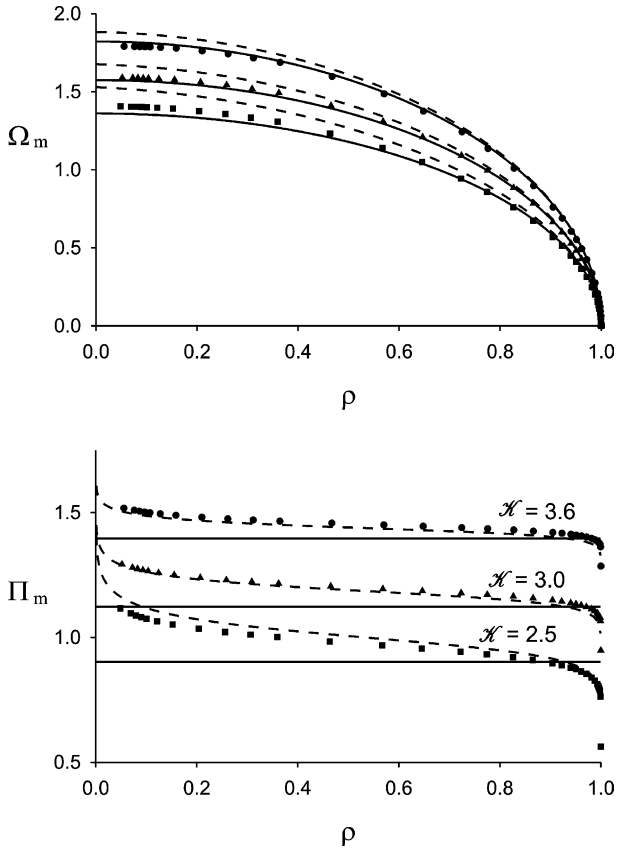

Fig. 5. Comparison of the opening and pressure of analytical solution and Loramec simulation given in the viscosity scaling for $\mathscr{K} = 2.5$, 3.0 and 3.6. The solid line corresponds to the zero-order solution and the dashed line corresponds to the first-order solution.

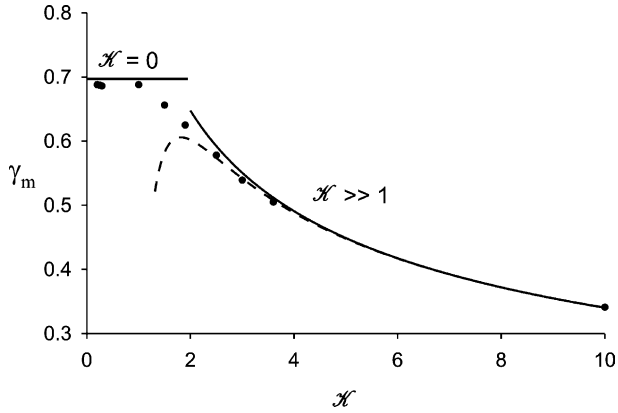

Fig. 6. Dependence of the dimensionless fracture radius in the viscosity scaling on the dimensionless toughness $\mathscr{K}$. The solid lines correspond to the zero-order solutions and the dashed line corresponds to the first-order solution.

The boundaries of the regimes of propagation are best determined from Fig. 6 showing the dependence of the fracture radius in the viscosity scaling, γ_m, on the toughness $\mathscr{K}$. The numerical results suggest that $\mathscr{K}_{m0} \simeq 1$ and $\mathscr{K}_{k0} \simeq 3.5$ (which is consistent with the estimate based on comparing the zero- and the first-order solution for large toughness). The transition regime appears to correspond to a remarkably small interval of $\mathscr{K}$.

The curve $\gamma_m(\mathscr{K})$, plotted in Fig. 6, is in principle travelled from left to right with increasing time. Although this result could be interpreted to mean that a radial fracture starts in the viscosity-dominated regime, it should be reminded that none of the solutions discussed here are applicable to the "early time" of fracture initiation. Indeed, the well radius has been assumed negligible compared to the fracture dimension. In fact, a radial fracture starts its existence in the toughness-dominated regime, matures in the viscosity-dominated regime, and ages back in the toughness-dominated regime.

It is of interest to estimate the times at which transitions between regimes of propagation occur, given realistic values of the parameters defining $\mathscr{K}$. Consider Table 6 listing typical ranges of values of those parameters. According to this table, the fracture would remain in the viscosity-dominated regime for many years if all the parameters assume average values. Although the viscosity-dominated regime would be over in a matter of seconds if all the parameters are set to extreme values in favor of toughness, it would still take several days before the toughness-dominated regime is reached (i.e., at least one order of magnitude longer than the duration of a hydraulic fracturing treatment). Further analysis shows that radial hydraulic fractures in impermeable rocks generally propagate in the viscosity regime, and that the toughness regime is relevant only in exceptional circumstances. This observation has profound consequences for the implementation of a propagation criterion in numerical simulators of hydraulic fractures.

Table 6
The typical values of the parameters

Quantity	Min–Max
Q (m^3/s)	0.03–0.08
E (GPa)	7–40
v	0.15–0.4
μ (Pa s)	0.1–0.5
K_{Ic} (MPa $m^{1/2}$)	0.5–2

7. Conclusions

One of the objectives of this research is to analyze the propagation regimes of a penny-shaped hydraulic fracture. Scaling of the equations reveals that this problem depends only on one dimensionless parameter, which can be chosen to be either the toughness $\mathscr{K}$ or the viscosity $\mathscr{M}$.

We have constructed the asymptotic solutions for $\mathscr{K} = 0$ and $\mathscr{K} \gg 1$. The zero toughness solution is characterized by a cubic root singularity of the pressure at the fracture tip. Due to the different nature of the singularity for $\mathscr{K} = 0$ and for $\mathscr{K} > 0$, this solution can be considered as an outer solution in a singular asymptotic expansion for small $\mathscr{K}$. The solution for large toughness is regular and can, in principle, be improved by considering higher order terms. In this case, the pressure is logarithmically singular near the tip, but this singularity is only revealed by the first-order approximation. Both the zero and large toughness solutions constitute new benchmarks which can be used to check numerical algorithm devised to model the propagation of planar hydraulic fractures of arbitrary shape.

The boundaries of the regimes of the propagation are analyzed by comparing the derived asymptotic solutions with the results of numerical simulations. First, it is shown that the numerical and asymptotic solutions indeed match for certain values of the controlling parameter. Then, the limit values of the parameter are estimated. According to these estimates, the fracture propagates in the viscosity-dominated regime if $\mathscr{K} \lesssim 1$ and in the toughness-dominated regime if $\mathscr{K} \gtrsim 3.5$. Finally, this analysis indicates that radial hydraulic fractures propagates in the viscosity-dominated regime (where toughness is irrelevant), for typical values of the physical parameters.

Acknowledgements

This research has been partially funded by the Graduate School of the University of Minnesota through the Doctoral Dissertation Fellowship awarded to AS, and by a grant from Schlumberger. This support is gratefully acknowledged. The authors would also like to thank Dr. Jean Desroches of Schlumberger for providing the results of the numerical simulations with Loramec; his general assistance to the research program in hydraulic fracturing at the University of Minnesota is also deeply appreciated.

Appendix A. Alternative form of the elasticity equation

The opening $w(r)$ of a radial crack due to the net pressure $p(r)$ is classically expressed as (Sneddon, 1951)

$$w(r) = \frac{8R}{\pi E'} \int_\rho^1 \frac{\xi}{\sqrt{\xi^2 - \rho^2}} \int_0^1 \frac{xp(x\xi R)}{\sqrt{1-x^2}} \,\mathrm{d}x\,\mathrm{d}\xi \tag{A.1}$$

where $\rho = r/R$. After operating the change of variable $s = x\xi$, the above equation is transformed into

$$w = \frac{8R}{\pi E'} \int_\rho^1 \frac{1}{\sqrt{\xi^2 - \rho^2}} \int_0^\xi \frac{s\bar{p}(s)}{\sqrt{\xi^2 - s^2}} \,\mathrm{d}s\,\mathrm{d}\xi \tag{A.2}$$

where $\bar{p}(r/R) \equiv p(r)$.

Following Barr (1991), the double integral in the right-hand side of (A.2) can be reduced to a single one. First, let us introduce the function $g(x, \xi)$

$$g(s, \xi) = \frac{s\bar{p}(s)}{\sqrt{\xi^2 - \rho^2}\sqrt{\xi^2 - s^2}} \tag{A.3}$$

Thus, (A.2) can be rewritten as

$$w = \frac{8R}{\pi E'} \int_\rho^1 \left[\int_0^\xi g(s,\xi)\,\mathrm{d}s \right] \mathrm{d}\xi \tag{A.4}$$

Changing the order of integration in the double integral of (A.4) yields

$$\int_\rho^1 \left[\int_0^\xi g(s,\xi)\,\mathrm{d}s \right] \mathrm{d}\xi = \int_0^\rho \left[\int_\rho^1 g(s,\xi)\,\mathrm{d}\xi \right] \mathrm{d}s + \int_\rho^1 \left[\int_s^1 g(s,\xi)\,\mathrm{d}\xi \right] \mathrm{d}s$$

Hence,

$$\begin{aligned} \int_\rho^1 \left[\int_0^\xi g(s,\xi)\,\mathrm{d}s \right] \mathrm{d}\xi = {} & \int_0^\rho s\bar{p}(s) \left[\int_\rho^1 \frac{1}{\sqrt{\xi^2-\rho^2}\sqrt{\xi^2-s^2}}\,\mathrm{d}\xi \right] \mathrm{d}s \\ & + \int_\rho^1 sp(\bar{s}) \left[\int_s^1 \frac{1}{\sqrt{\xi^2-\rho^2}\sqrt{\xi^2-s^2}}\,\mathrm{d}\xi \right] \mathrm{d}s \end{aligned} \tag{A.5}$$

The terms in the square brackets can be expressed in terms of F, the elliptic integral of the first kind (Abramowitz and Stegun, 1964)

$$\int_\rho^1 \frac{1}{\sqrt{\xi^2-\rho^2}\sqrt{\xi^2-s^2}}\,\mathrm{d}\xi = \frac{1}{\rho} F\left(\arcsin\sqrt{\frac{1-\rho^2}{1-s^2}}, \frac{s^2}{\rho^2} \right), \quad \text{if } \rho > s \tag{A.6}$$

$$\int_s^1 \frac{1}{\sqrt{\xi^2-\rho^2}\sqrt{\xi^2-s^2}}\,\mathrm{d}\xi = \frac{1}{s} F\left(\arcsin\sqrt{\frac{1-s^2}{1-\rho^2}}, \frac{\rho^2}{s^2} \right), \quad \text{if } s < \rho \tag{A.7}$$

The final expression for w is given by (40).

Appendix B. Regularization of the elasticity equation

The main difficulty in calculating the coefficients L_{ij} in (66) stems from a weak singularity in the kernel G. Rewrite (66) as

$$L_{ij} = \frac{8}{\pi} \int_0^1 \overline{\Omega}_i^*(\rho) I(j,\rho) \rho\,\mathrm{d}\rho$$

where

$$I(j,\rho) = \int_0^\rho \frac{1}{\rho} F\left(\arcsin\sqrt{\frac{1-\rho^2}{1-\xi^2}}, \frac{\xi^2}{\rho^2} \right) \Pi_j^*(\xi)\xi\,\mathrm{d}\xi + \int_\rho^1 \frac{1}{\xi} F\left(\arcsin\sqrt{\frac{1-\xi^2}{1-\rho^2}}, \frac{\rho^2}{\xi^2} \right) \Pi_j^*(\xi)\xi\,\mathrm{d}\xi \tag{B.1}$$

The complete elliptic function of the first kind, $F(\pi/2,\rho)$, behaves as (Abramowitz and Stegun, 1964)

$$F(\pi/2,\rho) \simeq \frac{1}{2} \ln\left(\frac{16}{1-\rho^2} \right), \quad \rho \to 1 \tag{B.2}$$

but here both arguments of the elliptic function F tend simultaneously to the singular point $(\pi/2, 1)$. The proper behavior can be derived, however, by asymptotic expansion of F

$$F\left(\arcsin\sqrt{\frac{1-\rho^2}{1-\xi^2}},\frac{\xi^2}{\rho^2}\right)\simeq\frac{1}{2}\ln\left(\frac{1-\rho}{1+\rho}\frac{16\rho^2}{\rho^2-\xi^2}\right),\quad \xi\to\rho \tag{B.3}$$

The new asymptote reveals a logarithmic singularity near $\rho=1$. After analyzing the singularity of the kernel, the integral (B.1) can be regularized in the usual way

$$\begin{aligned}I(j,\rho)=&\int_0^\rho\frac{1}{\rho}\left[F\left(\arcsin\sqrt{\frac{1-\rho^2}{1-\xi^2}},\frac{\xi^2}{\rho^2}\right)\Pi_j^*(\xi)\xi-\frac{1}{2}\ln\left(\frac{1-\rho}{1+\rho}\frac{16\rho^2}{\rho^2-\xi^2}\right)\Pi_j^*(\rho)\rho\right]\mathrm{d}\xi\\&+\int_\rho^1\left[F\left(\arcsin\sqrt{\frac{1-\xi^2}{1-\rho^2}},\frac{\rho^2}{\xi^2}\right)\Pi_j^*(\xi)-\frac{1}{2}\ln\left(\frac{1-\xi}{1+\xi}\frac{16\xi^2}{\xi^2-\rho^2}\right)\Pi_j^*(\rho)\right]\mathrm{d}\xi\\&+\frac{1}{2}\Pi_j^*(\rho)\int_0^\rho\ln\left(\frac{1-\rho}{1+\rho}\frac{16\rho^2}{\rho^2-\xi^2}\right)\mathrm{d}\xi+\frac{1}{2}\Pi_j^*(\rho)\int_\rho^1\ln\left(\frac{1-\xi}{1+\xi}\frac{16\xi^2}{\xi^2-\rho^2}\right)\mathrm{d}\xi\end{aligned} \tag{B.4}$$

After noting that the last two integrals in the above expression can be derived analytically and that

$$\int_\rho^1 F\left(\arcsin\sqrt{\frac{1-\xi^2}{1-\rho^2}},\frac{\rho^2}{\xi^2}\right)\mathrm{d}\xi=1-\rho \tag{B.5}$$

we can rewrite (B.4) as

$$\begin{aligned}I(j,\rho)=&\int_0^\rho\frac{1}{\rho}\left[F\left(\arcsin\sqrt{\frac{1-\rho^2}{1-\xi^2}},\frac{\xi^2}{\rho^2}\right)\Pi_j^*(\xi)\xi-\frac{1}{2}\ln\left(\frac{1-\rho}{1+\rho}\frac{16\rho^2}{\rho^2-\xi^2}\right)\Pi_j^*(\rho)\rho\right]\mathrm{d}\xi\\&+\int_\rho^1 F\left(\arcsin\sqrt{\frac{1-\xi^2}{1-\rho^2}},\frac{\rho^2}{\xi^2}\right)\left[\Pi_j^*(\xi)-\Pi_j^*(\rho)\right]\mathrm{d}s+\frac{1}{2}\Pi_j^*(\rho)\left[2+\rho\ln\frac{4(1-\rho)}{1+\rho}\right]\end{aligned} \tag{B.6}$$

The above integral can be easily calculated up to a given precision at any point, except close to the tip. In order to get an accurate value $I(j,\rho)$ near $\rho=1$, the known asymptote for the opening can be used to yield

$$I(j,\rho)\simeq\frac{\pi}{4}3^{3/2}\frac{G_{j-1}(\frac{4}{3},2,1)}{h_{j-1}^{1/2}(\frac{4}{3},2)}(1-\rho)^{2/3},\quad \rho\ll1 \tag{B.7}$$

Appendix C. Left and right hand sides of the lubrication equation at control points

The left and right hand sides of the lubrication equation are given respectively by

$$\Xi^l(\rho;A_1^{(n)},\ldots,A_n^{(n)},B^{(n)})=\left(\sum_{i=1}^{n+1}C_i^{(n)}I_i^*(\rho)+B^{(n)}I^{**}(\rho)\right)+\frac{4}{9}\rho^2\left(\sum_{i=1}^{n+1}C_i^{(n)}\Omega_i^*(\rho)+B^{(n)}\Omega^{**}(\rho)\right) \tag{C.1}$$

$$\Xi^r(\rho;A_1^{(n)},\ldots,A_n^{(n)},B^{(n)})=-\rho\left(\sum_{i=1}^{n+1}C_i^{(n)}\Omega_i^*(\rho)+B^{(n)}\Omega^{**}(\rho)\right)^3\left(\sum_{i=1}^{n}A_i^{(n)}\Pi_i^{*\prime}(\rho)+B^{(n)}\Pi^{**\prime}(\rho)\right) \tag{C.2}$$

where $I_i^*(\rho)$ and $I^{**}(\rho)$ are functions defined by

$$I_i^*=\int_\rho^1\Omega_i^*(\xi)\xi\,\mathrm{d}\xi,\quad I^{**}=\int_\rho^1\Omega^{**}(\xi)\xi\,\mathrm{d}\xi \tag{C.3}$$

Table 7
Integrals $I^{**}(\rho)$ and $I_i^*(\rho)$ for $i = 1, \ldots, 5$

$I^{**}(\rho)$	$-\frac{4}{9\pi}\left(-3\pi\rho^3 - 2\sqrt{1-\rho^2}(1-4\rho^2) + 6\rho^3 \arcsin\rho\right)$
$I_1^*(\rho)$	$-0.2092(1-\rho)^{2/3}(-3-2\rho+5\rho^2)$
$I_2^*(\rho)$	$0.02710(1-\rho)^{2/3}(9+6\rho+115\rho^2-130\rho^3)$
$I_3^*(\rho)$	$-0.001761(1-\rho)^{2/3}(-81-54\rho+2727\rho^2-9280\rho^3+6688\rho^4)$
$I_4^*(\rho)$	$-25.30\sqrt{2}(1-\rho)^{2/3}(\rho-1)(-0.2291-0.9529\rho+\rho^2)(0.01055+0.06145\rho+\rho^2)$
$I_5^*(\rho)$	$-87.92\sqrt{2}(1-\rho)^{2/3}(\rho-1)(\rho-0.6631)(\rho-0.5744)(\rho-0.06444)(0.02091-0.02217\rho+\rho^2)$

The integrals $I_i^*(\rho)$ can be derived analytically for any particular i (although the general form of the integral I_i^* has not been found). The explicit expressions for the first five integrals $I_i^*(\rho)$ and the integral $I^{**}(\rho)$ are given in Table 7.

The last term in the sum (67) has to be understood as a limit, because Ξ^l and Ξ^r are both zero at the tip. Consider the asymptotic behavior of the left and right hand sides of Eq. (43) near $\rho = 1$

$$\Xi^l(\rho; A_1^{(n)}, \ldots, A_n^{(n)}, B^{(n)}) \simeq \frac{4}{9}\overline{\Omega}_{m0}^{(n)} \tag{C.4}$$

$$\Xi^r(\rho; A_1^{(n)}, \ldots, A_n^{(n)}, B^{(n)}) \simeq -\left(\overline{\Omega}_{m0}^{(n)}\right)^3 \frac{\mathrm{d}\Pi_{m0}^{(n)}}{\mathrm{d}\rho} \tag{C.5}$$

In the limit when $\rho \to 1$ both Ξ^l and Ξ^r are zero, but their ratio is finite

$$\lim_{\rho\to 1} \frac{\Xi^r(\rho; A_1^{(n)}, \ldots, A_n^{(n)}, B^{(n)})}{\Xi^l(\rho; A_1^{(n)}, \ldots, A_n^{(n)}, B^{(n)})} = -\frac{9}{4}\lim_{\rho\to 1}\left[(\overline{\Omega}_{m0}^{(n)})^2 \frac{\mathrm{d}\Pi_{m0}^{(n)}}{\mathrm{d}\rho}\right] \tag{C.6}$$

Since $\overline{\Omega}_{m0}^{(n)}$ and $\Pi_{m0}^{(n)}$ have the following asymptotic expansions near the tip

$$\overline{\Omega}_{m0}^{(n)} = (1-\rho)^{2/3}\sum_{i=1}^{n+1} C_i^{(n)} \frac{G_{i-1}(\frac{10}{3}, 2, 1)}{h_{i-1}^{1/2}(\frac{10}{3}, 2)} + \mathrm{O}[(1-\rho)^{3/2}] \tag{C.7}$$

$$\Pi_{m0}^{(n)} = (1-\rho)^{-1/3}\sum_{i=1}^{n} A_i^{(n)} \frac{G_{i-1}(\frac{4}{3}, 2, 1)}{h_{i-1}^{1/2}(\frac{4}{3}, 2)} + \mathrm{O}(1) \tag{C.8}$$

Substitution of the above equations into the limit (C.6) yields

$$\lim_{\rho\to 1} \frac{\Xi^r(\rho; A_1^{(n)}, \ldots, A_n^{(n)}, B^{(n)})}{\Xi^l(\rho; A_1^{(n)}, \ldots, A_n^{(n)}, B^{(n)})} = -\frac{3}{4}\left(\sum_{i=1}^{n} A_i^{(n)} \frac{G_{i-1}(\frac{4}{3}, 2, 1)}{h_{i-1}^{1/2}(\frac{4}{3}, 2)}\right)\left(\sum_{i=1}^{n+1} C_i^{(n)} \frac{G_{i-1}(\frac{10}{3}, 2, 1)}{h_{i-1}^{1/2}(\frac{10}{3}, 2)}\right)^2$$

Hence the last term in the sum (67) is given by

$$\left[\frac{3}{4}\left(\sum_{i=1}^{n} A_i^{(n)} \frac{G_{i-1}\left(\frac{4}{3}, 2, 1\right)}{h_{i-1}^{1/2}\left(\frac{4}{3}, 2\right)}\right)\left(\sum_{i=1}^{n+1} C_i^{(n)} \frac{G_{i-1}\left(\frac{10}{3}, 2, 1\right)}{h_{i-1}^{1/2}\left(\frac{10}{3}, 2\right)}\right)^2 + 1\right]^2 \tag{C.9}$$

Appendix D. Evaluation of Ω_{k1} and ω_{k1}

Noting that Π_{k0} is a constant, the expression (79) for Ω_{k1} can be rewritten as

$$\Omega_{k1} = \frac{8}{\pi}\gamma_{k1}\Pi_{k0}\int_\rho^1 \frac{\xi}{\sqrt{\xi^2-\rho^2}}\int_0^1 \frac{x}{\sqrt{1-x^2}}\,\mathrm{d}x\,\mathrm{d}\xi + \frac{8}{\pi}\gamma_{k0}\int_\rho^1 \frac{\xi}{\sqrt{\xi^2-\rho^2}}\int_0^1 \frac{x\Pi_{k1}(x\xi)}{\sqrt{1-x^2}}\,\mathrm{d}x\,\mathrm{d}\xi \tag{D.1}$$

where $\Pi_{k1}(\rho)$ is given by (88). The following integrals are needed to evaluate Ω_{k1}

$$\int_\rho^1 \frac{\xi}{\sqrt{\xi^2-\rho^2}} \int_0^1 \frac{x}{\sqrt{1-x^2}}\,\mathrm{d}x\,\mathrm{d}\xi = \sqrt{1-\rho^2} \tag{D.2}$$

$$\int_\rho^1 \frac{\xi}{\sqrt{\xi^2-\rho^2}} \int_0^1 \frac{x\ln(x\xi)}{\sqrt{1-x^2}}\,\mathrm{d}x\,\mathrm{d}\xi = (\ln 2-2)\sqrt{1-\rho^2}+\rho\arccos\rho \tag{D.3}$$

$$\int_\rho^1 \frac{\xi}{\sqrt{\xi^2-\rho^2}} \int_0^1 \frac{x\ln(1-(x\xi)^2)}{\sqrt{1-x^2}}\,\mathrm{d}x\,\mathrm{d}\xi = 2I^*(\rho)-2\sqrt{1-\rho^2} \tag{D.4}$$

where the integral I^*, given below, has to be evaluated numerically

$$I^*(\rho) = \int_\rho^1 \frac{\sqrt{1-\xi^2}}{\sqrt{\xi^2-\rho^2}}\arcsin\xi\,\mathrm{d}\xi \tag{D.5}$$

The function $I^*(\rho)$ is plotted in Fig. 7.

Finally, integration of (D.1) yields

$$\Omega_{k1} = B_k\sqrt{1-\rho^2} - \frac{8}{\pi}A_k\gamma_{k0}\left[\left(\frac{\ln 2-2}{3}+\frac{2}{5}\right)\sqrt{1-\rho^2}+\frac{1}{3}\rho\arccos\rho-\frac{2}{5}I^*(\rho)\right] \tag{D.6}$$

where

$$B_k = \frac{8}{\pi}\left(\gamma_{k1}\Pi_{k0}+\gamma_{k0}\Pi^*_{k1}\right)$$

Determination of the volume ω_{k1} corresponding to the opening Ω_{k1} by means of (83) requires the following integrals

$$\int_0^1 \sqrt{1-\rho^2}\rho\,\mathrm{d}\rho = \frac{1}{3},\quad \int_0^1 \arccos\rho\rho^2\,\mathrm{d}\rho = \frac{2}{9},\quad \int_0^1 I^*(\rho)\rho\,\mathrm{d}\rho = \frac{2}{9} \tag{D.7}$$

Note that the last integral can be evaluated in closed form.

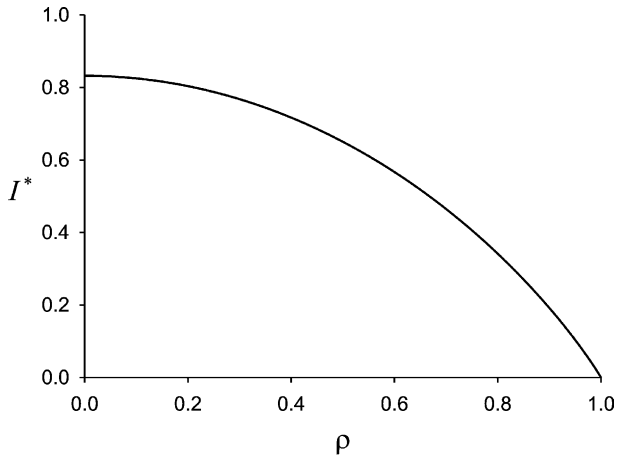

Fig. 7. Function I^*.

Finally, ω_{k1} can be expressed as

$$\omega_{k1} = \frac{2\pi}{3} B_k - \frac{16}{9} A_k \gamma_{k0} \left(\ln 2 - \frac{14}{15} \right) \tag{D.8}$$

References

Abé, H., Keer, L.M., Mura, T., 1979. Theoretical study of hydraulically fractured penny-shaped cracks in hot, dry rocks. Int. J. Numer. Anal. Meth. Geomech. 3, 79–96.

Abé, H., Mura, T., Keer, L.M., 1976. Growth rate of a penny-shaped crack in hydraulic fracturing of rocks. J. Geophys. Res. 81, 5335–5340.

Abramowitz, M., Stegun, I.A. (Eds.), 1964. Handbook of Mathematical Functions with Formulas, Graphs, and Mathematical Tables. Applied Mathematics Series, 55. US Govt. Print. Off, Washington, DC.

Advani, S.H., Torok, J.S., Lee, J.K., Choudhry, S., 1987. Explicit time-dependent solutions and numerical evaluations for penny-shaped hydraulic fracture models. J. Geophys. Res. 92 (B8), 8049–8055.

Advani, S.H., Lee, T.S., Lee, J.K., 1990. Three dimensional modeling of hydraulic fractures in layered media: finite element formulations. ASME J. Energy Res. Tech. 112, 1–18.

Barenblatt, G.I., 1956. On the formation of horizontal cracks in hydraulic fracture of an oil-bearing stratum. Prikl. Mat. Mech. 20, 475–486.

Barr, D.T., 1991. Leading-edge analysis for correct simulation of interface separation and hydraulic fracturing. Ph.D. thesis, Massachusetts Institute of Technology, Cambridge, MA.

Batchelor, G.K., 1967. An Introduction to Fluid Dynamics. Cambridge University Press, Cambridge, UK.

Carbonell, R., Desroches, J., Detournay, E., 1999. A comparison between a semi-analytical and a numerical solution of a two-dimensional hydraulic fracture. Int. J. Solids Struct. 36 (31–32), 4869–4888.

Clifton, R.J., Abou-Sayed, A.S., 1981. A variational approach to the prediction of the three-dimensional geometry of hydraulic fractures. In: Proceedings of the SPE/DOE Low Permeability Reservoir Symposium, Denver, SPE 9879.

Desroches, J., 2000. Personal communication.

Desroches, J., Thiercelin, M., 1993. Modeling propagation and closure of micro-hydraulic fractures. Int. J. Rock Mech. Min. Sci. 30, 1231–1234.

Desroches, J., Detournay, E., Lenoach, B., Papanastasiou, P., Pearson, J.R.A., Thiercelin, M., Cheng, A.H.-D., 1994. The crack tip region in hydraulic fracturing. Proc. Roy. Soc. London, Ser. A (447), 39–48.

Detournay, E., 1999. Fluid and solid singularities at the tip of a fluid-driven fracture. In: Durban, D., Pearson, J. (Eds.), Proceedings of the IUTAM Symposium on Non-Linear Singularities in Deformation and Flow, Haifa. Kluwer Academic Publishers, Dordrecht, pp. 27–42.

Garagash, D., 2000. Hydraulic fracture propagation in elastic rock with large toughness. In: Girard, J., Liebman, M., Breeds, C., Doe, T. (Eds.), Rock Around the Rim—Proceedings of the Fourth North American Rock Mechanics Symposium. Balkema, Rotterdam, pp. 221–228.

Garagash, D.I., Detournay, E., 2000. The tip region of a fluid-driven fracture in an elastic medium. ASME J. Appl. Mech. 67, 183–192.

Geertsma, J., de Klerk, F., 1969. A rapid method of predicting width and extent of hydraulic induced fractures. JPT 246, 1571–1581.

Geertsma, J., Haafkens, R., 1979. A comparison of the theories for predicting width and extent of vertical hydraulically induced fractures. ASME J. Energy Res. Tech. 101, 8–19.

Kanninen, M.F., Popelar, C.H., 1985. Advanced Fracture Mechanics. In: volume 15 of The Oxford Engineering Science Series. Oxford University Press, Oxford, UK.

Khristianovic, S., Zheltov, Y., 1955. Formation of vertical fractures by means of highly viscous fluids. In: Proceedings of the Fourth World Petroleum Congress, Rome, vol. II, pp. 579–586.

Mendelsohn, D.A., 1984. A review of hydraulic fracture modeling—part i: General concepts, 2d models, motivation for 3d modeling. ASME J. Energy Res. Tech. 106, 369–376.

Nordgren, R., 1972. Propagation of vertical hydraulic fractures. J. Pet. Tech. 253, 306–314 (SPE 3009).

Peirce, A.P., Siebrits, E., 2001. The Scaled Flexibility Matrix Method for the efficient solution of boundary value problems in 2D and 3D layered elastic media. Comp. Meth. Appl. Mech. Eng. 190, 5935–5956.

Perkins, T.K., Kern, L.R., 1961. Widths of hydraulic fractures. J. Pet. Tech., Trans. AIME 222, 937–949.

Rice, J.R., 1968. Mathematical analysis in the mechanics of fracture. In: Liebowitz, H. (Ed.), Fracture, an Advanced Treatise, vol. II. Academic Press, New York, NY, pp. 191–311 (Chapter 3).

Shah, K.R., Carter, B.J., Ingraffea, A.R., 1997. Hydraulic fracturing simulation in parallel computing environments. Int. J. Rock Mech. Min. Sci. 34 (3/4), 474.

Siebrits, E., Peirce, A.P., 2002. An efficient multi-layer planar 3D fracture growth algorithm using a fixed mesh approach. Int. J. Numer. Meth. Engng. 53, 691–717.

Sneddon, I.N., 1951. Fourier Transforms. McGraw-Hill, New York, NY.

Sousa, J.L.S., Carter, B.J., Ingraffea, A.R., 1993. Numerical simulation of 3D hydraulic fracture using Newtonian and power-law fluids. Int. J. Rock Mech. Min. Sci. 30 (7), 1265–1271.

Spence, D.A., Sharp, P.W., 1985. Self-similar solution for elastohydrodynamic cavity flow. Proc. Roy. Soc. London, Ser. A (400), 289–313.

Warpinski, N.R., Moschovidis, Z.A., Parker, C.D., Abou-Sajed, I.S., 1993. Comparison study of hydraulic fracturing models: Test case GRI-staged field experiment No. SPE, pp. 469–478.